

Quantum computing with quantum-dot cellular automata

Géza Tóth* and Craig S. Lent†

Department of Electrical Engineering, University of Notre Dame, Notre Dame, Indiana 46556

(Received 23 February 2000; published 19 April 2001)

Quantum-dot cellular automata (QCA), arrays of coupled quantum-dot devices, are proposed for quantum computing. The notion of coherent QCA (CQCA) is introduced in order to distinguish QCA applied to quantum computing from classical digital QCA. Information is encoded in the spatial state of the electrons in the multidot system. A line of CQCA cells can work as a quantum register. The basic single- and multi-qubit operations can be realized by pulses given to the cell electrodes.

DOI: 10.1103/PhysRevA.63.052315

PACS number(s): 03.67.Lx, 02.70.-c, 85.35.Be, 85.35.Gv

I. INTRODUCTION

Quantum computing [1–40] has attracted attention in the past two decades because it was found that computers exploiting quantum mechanics are able to outperform classical digital computers in certain areas (factoring integers [33], searching [7,36], etc.). Beside designing and analyzing new quantum computing algorithms, significant effort has been made to find a suitable realization for a quantum computer. With the application of nuclear magnetic resonance (NMR), several groups have created quantum computers [10–19] up to seven qubits in size. Other implementations employ ion traps [34], cavity QED [35], Josephson junctions [37–40], and semiconductor quantum dots [20,25–32].

We propose a multiple-quantum-dot structure, quantum-dot cellular automata (QCA) [41–49], and investigate the basic quantum gates suitable for this implementation. Information is encoded in the position of the electrons inside the QCA cell. The basic single- and multi-qubit operations can be realized by lowering and raising the interdot tunneling barriers. Several other realizations have been proposed using semiconductor quantum dots. The information can be encoded in the electron spin [26,32], in the position of the electron in the double dot [25,31], or the ground state and excited state of the electron can be used for logical “0” and “1” [28,30]. The quantum computing algorithms are performed by manipulating the interdot coupling with magnetic field [26], optically by laser pulses [25,26,30] or by using external electrodes to raise and lower the interdot barriers [26,31,32].

The QCA concept [41–49] was originally proposed as a transistorless alternative for digital circuit technology at nanoscale. A QCA cell consists of four quantum dots as shown in Fig. 1(a). The lines in the diagram indicate the possibility of interdot tunneling. The cell has two allowed charge polarizations, $P = +1$ and -1 , since the two extra electrons occupy antipodal sites [Fig. 1(b)]. When placed in close proximity along a line, QCA cells align with the same

polarization. In addition to the cell line, logical gates [44] and memory [50] can also be realized. Recently, experiments were done that implemented QCA cells with metal islands [51,52] as a single-electron tunneling circuit [53]. A semiconductor realization is also being developed [56–59]. QCA cells used for classical computing applications are mostly fully polarized during the operation. Dissipation plays a positive role helping the system to stay near the ground state.

Our aim here is to explore the possibilities of using semiconductor QCA for quantum computing [60]. In the case of quantum computing, the cells are not fully polarized: they can be in a superposition of the $P = +1$ and -1 basis states. Similarly, a cell line can be in a superposition of the multi-qubit product states. Unlike classical digital applications, quantum computing ideally needs coherence for correct operation. (In real systems, decoherence is always present, thus its effects must be circumvented by error correction.) In order to distinguish QCA applied for quantum computing from the classical digital QCA, the notion of coherent QCA (CQCA) will be used.

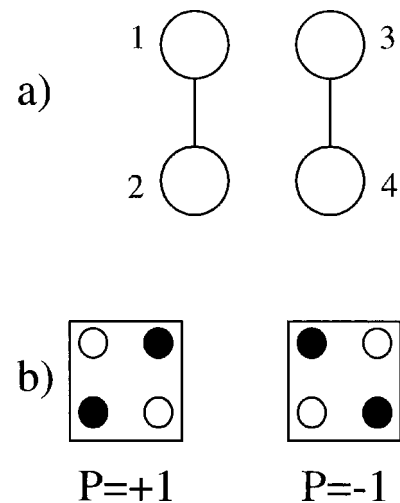


FIG. 1. Schematic of the basic four-site semiconductor QCA cell. (a) The geometry of the cell. The lines indicate the possibility of interdot tunneling. The tunneling energy between two sites (quantum dots) is determined by the heights of the potential barrier between them. (b) Coulombic repulsion causes the two electrons to occupy antipodal sites within the cell. These two bistable states result in cell polarization of $P = +1$ and -1 .

*Present address: Theoretical Physics, University of Oxford, 1 Keble Road, Oxford OX1 3NP, United Kingdom. Email address: Geza.Toth.17@nd.edu

†Author to whom correspondence should be addressed. Email address: Craig.S.Lent.1@nd.edu

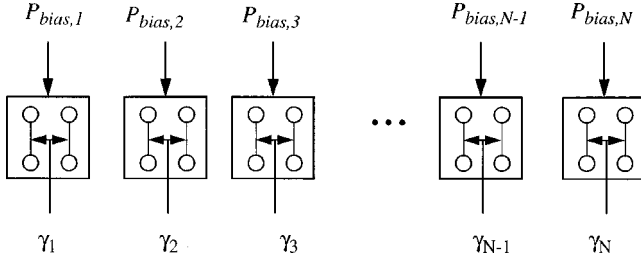


FIG. 2. The N -qubit register realized with a line of N CQCA cells. Each cell has two inputs: the γ_j interdot tunneling energy and the $P_{\text{bias},j}$ bias polarization.

In Sec. II, the CQCA cell line is used as a quantum register. In Secs. III and IV, the single- and multi-qubit operations are presented. In Sec. V, the decoherence and other issues pertaining to the physical realization are discussed.

II. THE CQCA CELL LINE AS A QUANTUM REGISTER

An N -qubit register can be realized with a line of N CQCA cells as shown in Fig. 2. The γ_j tunneling energy is set by external electrodes that lower or raise the interdot barriers of the j th cell. A cell can be turned off by lowering the barriers. (When a cell's barriers are extremely low, it does not have a definite polarization and it does not affect its neighbors.) Each cell is Coulombically coupled to its left and right neighbors and to the bias electrodes. The biases, $P_{\text{bias},j}$, are set externally, thus these and the γ_j 's are the inputs of the quantum register [54].

There are three main steps when executing a program on the quantum register: writing in the initial state, running the algorithm, and reading out the final state. The initial state can be loaded into the register by setting the biases to $|P_{\text{bias},j}| \gg 1$ and waiting for a time sufficient to settle in the ground state. If $P_{\text{bias},j} \gg 1$ ($P_{\text{bias},j} \ll -1$), then the cell is forced to the $P = +1$ ($P = -1$) state. The execution of the algorithm is realized with a series of pulses applied to the electrodes of the cell. The final state can be read out by electrometers that are sensitive enough to detect the presence or the absence of an electron (e.g., single electron transistor [52,53]).

In [48], a simple Hamiltonian of an extended Hubbard type was used to describe the cell. The relatively weak spin-spin interaction between electrons in different dots is ignored. Each quantum dot is considered as a site, internal degrees of freedom being thus ignored. The Hamiltonian employed is given by

$$\hat{H} = \sum_{i,\sigma} (E_{\text{on-site}} + V_i) \hat{n}_{i,\sigma} + \sum_{i>j,\sigma} t_{i,j}^\dagger (\hat{a}_{i,\sigma} \hat{a}_{j,\sigma} + \hat{a}_{j,\sigma}^\dagger \hat{a}_{i,\sigma}) + \sum_i E_Q \hat{n}_{i,\uparrow} \hat{n}_{i,\downarrow} + \sum_{i>j,\sigma,\sigma'} V_Q \frac{\hat{n}_{i,\sigma} \hat{n}_{i,\sigma'}}{|R_{ij}|}. \quad (1)$$

Here we use the usual second quantized notation where $\hat{a}_{i,\sigma}$ ($\hat{a}_{i,\sigma}^\dagger$) annihilates (creates) an electron on site i with spin σ . The number operator for electrons of spin σ on site i is $\hat{n}_{i,\sigma} = \hat{a}_{i,\sigma}^\dagger \hat{a}_{i,\sigma}$. In Eq. (1), the first term represents the on-site energy of each dot. The potential energy of an electron at dot

i due to charges outside the cell, including effects of charges in other cells and the bias electrodes, is V_i . The second term accounts for the electron tunneling between sites, with $t_{i,j} = t$ for vertical neighbors and $t_{ij} = 0$ for horizontal neighbors and antipodal sites. The third term is the on-site charging cost to put two electrons of opposite spin on the same dot. The last term corresponds to the Coulombic interaction between electrons on different sites within a cell.

Assuming that both double dots have one electron, and the electrons stay in the ground state of the dot, the cell state is a superposition of four basis states: $|TB\rangle$, $|BT\rangle$, $|TT\rangle$, and $|BB\rangle$. Here T (B) indicates that the electron is in the top (bottom) dot. If the E_{DD} electrostatic coupling energy between the double dots inside the cell is much larger than both the energy of the coupling to the neighboring cells and the t tunneling energy, then the diagonal elements in the Hamiltonian corresponding to the $|TT\rangle$ and $|BB\rangle$ states are relatively large. Consequently, these states have a very small amplitude during the dynamics. The system can be considered as a two-state system with the basis states $|TB\rangle$ and $|BT\rangle$ [55]. Note that state transition happens only through $|TT\rangle$ and $|BB\rangle$. Standard second-order perturbation theory leads to an effective tunneling energy $\gamma \approx 2t^2/E_{\text{DD}}$ between the two basis states, where E_{DD} is the energy cost of having both electrons of the cell either on the top or on the bottom dots ($E_{\text{DD}} = \langle TT | \hat{H} | TT \rangle - \langle BT | \hat{H} | BT \rangle$, $t = \langle TT | \hat{H} | TB \rangle$).

A double-dot cell clearly fits the two-state description, however for double-dot cells (dipoles) the electrostatic coupling decreases with the third power of the distance, thus next-to-nearest-neighbor coupling cannot be ignored. [For four-dot cells (quadrupoles), the strength of the coupling decreases with the fifth power of the distance, thus next-to-nearest-neighbor coupling can be neglected.] The following deduction would be otherwise the same for double-dot cells, with the tunneling energy γ equal to the physical interdot tunneling energy t .

The Hamiltonian for a line of N CQCA cells, modeled as coupled two-state systems, is

$$\hat{H} = - \sum_{j=1}^N \gamma_j \hat{\sigma}_x(j) - \sum_{j=1}^{N-1} E_j \hat{\sigma}_z(j) \hat{\sigma}_z(j+1) + \sum_{j=1}^N E_0 P_{\text{bias},j} \hat{\sigma}_z(j). \quad (2)$$

The first term describes the tunneling between the $P = +1$ and -1 states. The second term describes the intercell electrostatic coupling. The third one couples the cells to external bias electrodes. E_j is the strength of Coulombic coupling between the j th and the $(j+1)$ st cell. It is positive since QCA cells tend to align. [For double-dot cells, E_j is negative since the cells tend to antialign, and an extra term appears in Eq. (2) describing the next-to-nearest-neighbor couplings [62].] For reasons explained later, E_j is alternating between E_0 and $2E_0$:

$$E_j = \begin{cases} E_0 & \text{if } j \text{ is odd} \\ 2E_0 & \text{if } j \text{ is even.} \end{cases} \quad (3)$$

Hamiltonian (2) is isomorphic to that of an Ising spin chain in a transverse magnetic field. The E_j and γ_j terms play the role of the interaction energy and the transverse magnetic-field strength, respectively. The γ_j and $P_{\text{bias},j}$ are settable, however the E_j intercell coupling is constant.

The polarization of the j th cell can be obtained as the expectation value of the $\hat{\sigma}_z$ operator:

$$P_j = -\langle \hat{\sigma}_z(j) \rangle. \quad (4)$$

With the minus sign, we follow the convention of Ref. [61] in defining the Pauli spin matrices:

$$\hat{\sigma}_x = \begin{bmatrix} 0 & 1 \\ 1 & 0 \end{bmatrix}, \quad \hat{\sigma}_y = \begin{bmatrix} 0 & i \\ -i & 0 \end{bmatrix}, \quad \hat{\sigma}_z = \begin{bmatrix} -1 & 0 \\ 0 & 1 \end{bmatrix}. \quad (5)$$

It is possible to construct an effective Schrödinger equation for a single cell using the mean-field approximation (see Ref. [47]; these equations can be obtained from the Hartree-Fock approximation applied to the CQCA line as a many-electron system):

$$\hat{H} = -\gamma \hat{\sigma}_x + E_\Sigma \hat{\sigma}_z, \quad (6)$$

where

$$E_\Sigma = E_{\text{left}} P_{\text{left}} + E_{\text{right}} P_{\text{right}} + E_0 P_{\text{bias}}, \quad (7)$$

The cell is coupled to its left and right neighbors through $E_{\text{left}} P_{\text{left}}$ and $E_{\text{right}} P_{\text{right}}$. (One of E_{left} and E_{right} is E_0 , the other is $2E_0$.) The edge cells do not have left or right neighbors, thus for them the corresponding polarizations are taken to be zero.

The state vector of a cell can be given as the linear combination of the fully polarized $P = +1$ and -1 basis states [see Fig. 1(b)]:

$$|\Psi\rangle = \alpha |1\rangle + \beta |-1\rangle = \begin{bmatrix} \alpha \\ \beta \end{bmatrix}. \quad (8)$$

Thus the state of a cell is described by two complex numbers, α and β .

The density matrix can also be used to describe the state of a single cell. The main advantage of the density matrix is that it can be used to describe energy dissipation, although such dissipation will not be considered now. The dynamics of the density matrix are given by the Liouville equation,

$$i\hbar \frac{\partial}{\partial t} \hat{\rho} = [\hat{H}, \hat{\rho}]. \quad (9)$$

The density matrix can be expressed as the linear combination of the $SU(2)$ generators, which are the Pauli spin matrices and the unit matrix:

$$\hat{\rho} = \frac{1}{2} (\hat{1} + \lambda_x \hat{\sigma}_x + \lambda_y \hat{\sigma}_y + \lambda_z \hat{\sigma}_z). \quad (10)$$

where $\lambda_a = \langle \hat{\sigma}_a \rangle$ for $a = x, y, z$. It can be seen from Eq. (10) that the three real λ_a values contain the same information about the quantum-mechanical state as the 2×2 density matrix does. In other words, although the density matrix has four complex (eight real) elements, it has only three (real) degrees of freedom, due to the constraints of Hermiticity and unit trace. The $\vec{\lambda}$ vector constructed from the three λ_a values is called the *coherence vector* (or the Bloch vector). The fully polarized $P = +1$ state corresponds to $\vec{\lambda} = [0, 0, -1]^T$ and the $P = -1$ state corresponds to $\vec{\lambda} = [0, 0, +1]^T$. In general, the third coordinate of $\vec{\lambda}$ equals $-P$.

The dynamical equation of the coherence vector is given as [61]

$$\frac{d\vec{\lambda}}{dt} = \vec{\Gamma} \times \vec{\lambda}, \quad (11)$$

where the cross denotes a vector product and $\Gamma_i = \text{Tr}(\hat{\sigma}_i \hat{H})$ for $i = x, y, z$. [\hat{H} is given in Eq. (6).] For the CQCA cell, $\vec{\Gamma}$ is

$$\hbar \vec{\Gamma} = \begin{bmatrix} -2\gamma \\ 0 \\ 2E_\Sigma \end{bmatrix}. \quad (12)$$

Equation (11) describes the precession of the coherence vector around $\vec{\Gamma}$. If there is no dissipation or decoherence, the length of the coherence vectors remains unity. In the case of dissipation, further terms are added to the right-hand side of Eq. (11). The coherence vector describes the state of the cell, while $\vec{\Gamma}$ represents the influence of the environment. $\vec{\Gamma}_x$ depends on the barrier height. $\vec{\Gamma}_z$ represents the coupling to the bias cell and to the neighbors.

If there is no entanglement during the operation (the register remains in a quantum-mechanical product state), then the mean-field description gives the same dynamics for the coherence vector as the model with the many-body Hamiltonian does [63].

Besides the coherence vector description, the quantum gates presented here will also be given by the unitary time evolution matrices computed from the many-cell Hamiltonian of the gates. They fully describe the functionality of the gate; the coherence vector description is useful for making the design of quantum gates clearer.

III. SINGLE-QUBIT ROTATIONS

We consider the elementary single-qubit rotations in λ space. If $\gamma \gg E_0$ (the barriers are low) and $P_{\text{bias}} = 0$, then $\hbar \vec{\Gamma} \cong [-2\gamma, 0, 0]^T$, which causes $\vec{\lambda}$ to precess around the $-x$ axis as shown in Fig. 3. (It is assumed that $\gamma = 0$ for all the other cells.) The duration of the precession corresponding to a rotation by an angle φ is

$$\Delta t = \frac{\varphi}{|\vec{\Gamma}|} = \frac{\hbar}{2\gamma} \varphi. \quad (13)$$

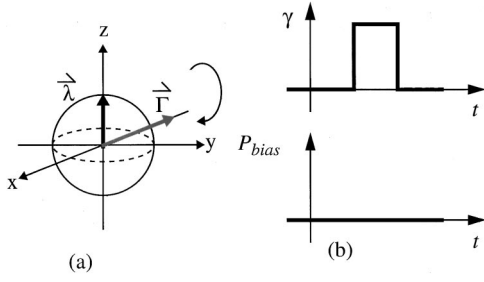


FIG. 3. Rotation around the $-x$ axis. (a) The rotation in the λ space. $\gamma \gg E_k$ (the barriers are low) and $P_{\text{bias}}=0$, thus $\hbar\vec{\Gamma} = [-2\gamma, 0, 0]^T$. (b) The pulses applied to the γ and the P_{bias} cell inputs.

The unitary time evolution operator for this single-qubit rotation is

$$U_{-x,\varphi} = e^{i\hat{\sigma}_x(\varphi/2)} = \begin{bmatrix} \cos \frac{\varphi}{2} & i \sin \frac{\varphi}{2} \\ i \sin \frac{\varphi}{2} & \cos \frac{\varphi}{2} \end{bmatrix}. \quad (14)$$

If $\varphi = \pi$, then the polarization of the cell is inverted, that is, the cell goes from the $\vec{\lambda} = [0, 0, +1]^T$ state to the $[0, 0, -1]^T$ state and vice versa, realizing the NOT operation, as shown in Fig. 4.

Another type of single-qubit rotation can be realized if $\gamma = 0$ (the barriers are high) and $P_{\text{bias}} \gg 1$. In this case, $\hbar\vec{\Gamma} \cong [0, 0, 2E_0P_{\text{bias}}]^T$, which causes $\vec{\Gamma}$ to precess around the z axis as shown in Fig. 5. The duration of precession corresponding to a rotation by an angle φ is

$$\Delta t = \frac{\varphi}{|\vec{\Gamma}|} = \frac{\hbar}{2E_0P_{\text{bias}}} \varphi. \quad (15)$$

The unitary time evolution operator for rotations around the z axis is

$$U_{z,\varphi} = e^{-i\hat{\sigma}_z(\varphi/2)} = \begin{bmatrix} e^{i(\varphi/2)} & 0 \\ 0 & e^{-i(\varphi/2)} \end{bmatrix}. \quad (16)$$

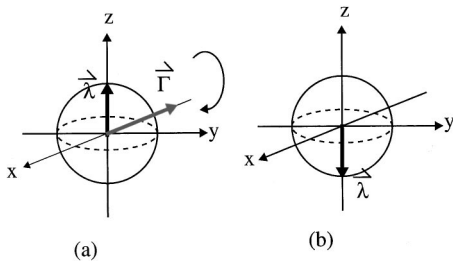


FIG. 4. NOT operation. (a) The initial state is $\vec{\lambda} = [0, 0, +1]^T$, that is, $P = -1$. (b) The final state obtained after 180° rotation around the x axis in the negative direction is $\vec{\lambda} = [0, 0, -1]^T$, that is, $P = +1$.

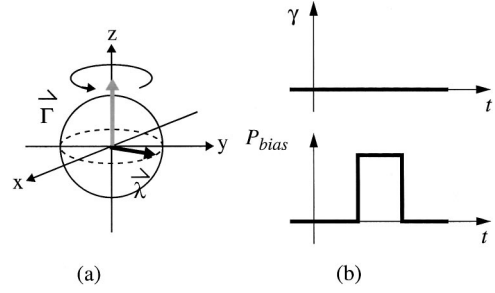


FIG. 5. Rotation around the z axis. (a) The rotation in the λ space. $P_{\text{bias}} \gg 1$ and $\gamma = 0$ (the barriers are high), thus $\hbar\vec{\Gamma} = [0, 0, 2E_0P_{\text{bias}}]^T$. (b) The pulses applied to the γ and the P_{bias} cell inputs.

The Hamiltonian (2) does not contain $\hat{\sigma}_y$, however the rotation around the y axis can still be realized by a series of rotations around the z and x axes:

$$\begin{aligned} U_{y,\varphi} &= U_{z,\pi/2} U_{-x,\varphi} U_{z,3\pi/2} \\ &= - \begin{bmatrix} \cos \frac{\varphi}{2} & -\sin \frac{\varphi}{2} \\ \sin \frac{\varphi}{2} & \cos \frac{\varphi}{2} \end{bmatrix} \\ &= -e^{i\hat{\sigma}_y(\varphi/2)}. \end{aligned} \quad (17)$$

The gates presented above were operating on a single qubit. It is reasonable to require that the state of the other qubits in the register do not change. This requirement can be fulfilled in the case of two-state systems by turning off the E_j intercell coupling for the rest of the cell line, however for the QCA register the coupling is constant. The unused part of the register will undergo time evolution, thus the effect of this time evolution must be examined. The time that would be necessary for the intercell coupling to affect the dynamics considerably is $T_{\text{coupling}} = \hbar/E_0$. In the case of single-qubit rotations, the duration of the operation is much shorter than that [compare T_{coupling} to Eq. (13) with the condition $\gamma \gg E_0$, and to Eq. (15) with the condition $P_{\text{bias}} \gg 1$], thus the change of the state in the rest of the line is negligible for single-qubit operations.

IV. MULTI-QUBIT OPERATIONS

In this section, we examine the multi-qubit operations possible with the Hamiltonian (2). The scheme for three-qubit operations presented here can be seen in Fig. 6. The middle cell (cell no. 2) is the *target* cell, its two neighbors (cell no. 1 and cell no. 3) are the left and right *control* cells. The polarizations of the control cells determine what happens to the target cell during the operation. In regard to the multi-qubit operations, $\vec{\lambda}$, $\vec{\Gamma}$, γ , P_{bias} , and E_Σ without indices refer to the target cell. The bias of both control cells are zero and their barriers are high.

For the three-qubit operations $0 < \gamma \ll E_0$. Depending on E_Σ , there are two possibilities for the time evolution of the target cell.

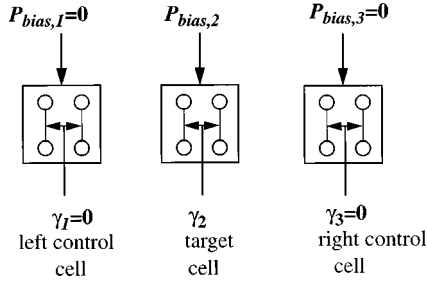


FIG. 6. Schematic of the arrangement for three-qubit operations. The polarizations of the control cells determine what happens to the target cell during the operation.

(i) If $E_\Sigma = 0$, then $\hbar\vec{\Gamma} = [-2\gamma, 0, 0]^T$, which causes $\vec{\lambda}$ to precess around the $-x$ axis.

(ii) If $E_\Sigma \neq 0$, then $\hbar\vec{\Gamma} \cong [0, 0, 2E_0P_{\text{bias}}]^T$, which causes $\vec{\lambda}$ to precess around the z axis.

For simplicity, suppose that $E_{\text{left}} = E_0$ and $E_{\text{right}} = 2E_0$. Substituting that into Eq. (7), one obtains

$$E_\Sigma = E_0(P_{\text{left}} + 2P_{\text{right}} + P_{\text{bias}}). \quad (18)$$

Let us examine the behavior of the target cell for the four possible cases when its two neighbors are fully polarized. E_Σ can be zero only for one of the four possible combinations of P_{left} and P_{right} . For example, choosing $P_{\text{bias}} = -3$, it is zero only if both P_{left} and P_{right} are $+1$. [The other three possibilities can be selected by $P_{\text{bias}} = -1, 1, \text{ and } 3$. Notice that if

TABLE I. The values of $\hbar\vec{\Gamma}$ for the four possible binary states of the left and right neighbors if $P_{\text{bias}} = -3$. If both P_{left} and P_{right} are $+1$, then $\vec{\Gamma}$ points in the $-x$ direction. If either of them is -1 , then $\vec{\Gamma}$ points in the $-z$ direction.

P_{left}	P_{right}	E_Σ/E_0	$\hbar\vec{\Gamma}$
-1	-1	-6	$[-2\gamma, 0, -12E_0]^T \approx [0, 0, -12E_0]^T$
-1	$+1$	-2	$[-2\gamma, 0, -4E_0]^T \approx [0, 0, -4E_0]^T$
$+1$	-1	-4	$[-2\gamma, 0, -8E_0]^T \approx [0, 0, -8E_0]^T$
$+1$	$+1$	0	$[-2\gamma, 0, 0]^T$

the E_j coupling would not alternate according to Eq. (3), then the $P_{\text{left}} = +1/P_{\text{right}} = -1$ case could not be distinguished from $P_{\text{left}} = -1/P_{\text{right}} = +1$ since $E_\Sigma = E_0(P_{\text{left}} + P_{\text{right}} + P_{\text{bias}})$ would be the same for both.]

Table I shows E_Σ and $\hbar\vec{\Gamma}$ for the four possible states of the neighbors assuming $P_{\text{bias}} = -3$. If both P_{left} and P_{right} are $+1$, then the coherence vector of the cell is rotated around the $-x$ axis, otherwise it is rotated around the $-z$ axis. This will be called *conditional rotation* in the following.

If the left or right neighbors are not fully polarized, then the time evolution of the three cells leads to entanglement and the mean-field-type description of Eqs. (11) and (12) can no longer be used. In this general case, the three-qubit gate corresponding to $P_{\text{bias}} = -3$ can be characterized by a unitary time evolution operator:

$$\hat{U} = \begin{bmatrix} 000 & 001 & 010 & 011 & 100 & 101 & 110 & 111 \\ e^{i(3\varphi_z/2)} & 0 & 0 & 0 & e^{i(\varphi_z/2)} & 0 & 0 & 0 \\ 0 & e^{-i(\varphi_z/2)} & 0 & 0 & 0 & \cos(\varphi_{-x}/2) & 0 & i \sin(\varphi_{-x}/2) \\ 0 & 0 & e^{-i(3\varphi_z/2)} & 0 & 0 & 0 & e^{-i(\varphi_z/2)} & 0 \\ 0 & 0 & 0 & e^{i(\varphi_z/2)} & 0 & i \sin(\varphi_{-x}/2) & 0 & \cos(\varphi_{-x}/2) \end{bmatrix} \begin{bmatrix} 000 \\ 001 \\ 010 \\ 011 \\ 100 \\ 101 \\ 110 \\ 111 \end{bmatrix} \quad (19)$$

In Eq. (19), φ_{-x} and φ_z are the angles of rotation around the $-x$ and z axes, respectively. They both depend on the t duration of the operation:

$$\varphi_{-x,t} = |\vec{\Gamma}|t = \frac{2\gamma}{\hbar}t \quad (20)$$

and

$$\varphi_{z,t} = |\vec{\Gamma}|t = \frac{2E_0}{\hbar}t. \quad (21)$$

The labels are showing the three-qubit states (the product basis vectors) corresponding to the rows and columns of the matrix. “1” and “0” refer to the $|1\rangle$ and $|-1\rangle$ states. The three digits correspond to the polarization of the left, the middle, and the right cells, respectively. Blank off-diagonal blocks refer to blocks of zeros omitted here for easier understanding.

Next, the rotation around the z axis will be eliminated. The rotation around z does not change the state of the target cell if φ_z is an integer multiple of 4π . The corresponding constraint for the duration of the operation is

$$t = \frac{2\pi\hbar}{E_0} m; \quad m = 0, 1, 2, \dots \quad (22)$$

With the choice of Eq. (22) for t , rotation occurs around the x axis when $P_{\text{left}} = P_{\text{right}}$, however the state of the cells do not change, if $P_{\text{left}} \neq P_{\text{right}}$. Thus φ_z can be omitted and φ_{-x} will be replaced with φ . Since t is constant, φ must be set by controlling γ . Combining Eqs. (20) and (22) gives

$$\gamma = \frac{\hbar}{2t} \varphi = \frac{E_0}{4\pi m} \varphi. \quad (23)$$

Applying condition (22) to Eq. (19), the following gate is obtained:

$$\hat{U}_{-x, \varphi; -3} = \begin{bmatrix} 1 & 0 & 0 & 0 \\ 0 & 1 & 0 & 0 \\ 0 & 0 & 1 & 0 \\ 0 & 0 & 0 & 1 \\ & 1 & 0 & 0 & 0 \\ & 0 & \cos \frac{\varphi}{2} & 0 & i \sin \frac{\varphi}{2} \\ & 0 & 0 & 1 & 0 \\ & 0 & i \sin \frac{\varphi}{2} & 0 & \cos \frac{\varphi}{2} \end{bmatrix}. \quad (24)$$

The “-3” refers to a rotation around x with the condition given by $P_{\text{bias}} = -3$. A variation of this quantum gate can be found in the literature [5,8] as U_λ or the Deutsch gate [15,23]. The only difference between Eq. (24) and the Deutsch gate is that cell no. 2 and cell no. 3 are exchanged. For $\phi = \pi$, the Deutsch gate realizes the Toffoli gate, with an additional $\pi/2$ phase shift if the target qubit is inverted. The Deutsch gate makes universal quantum computing possible.

It follows from Eq. (20) that the execution time of a multi-qubit gate is

$$t \sim \frac{\hbar}{2\gamma}. \quad (25)$$

Since $\gamma \ll E_0$, the execution time of Eq. (25) is much longer than $T_{\text{coupling}} = \hbar/E_0$. The other drawback of implementing the $\hat{U}_{-x, \varphi; -3}$ gate this way is that it requires an extremely accurate control [64] of the driver polarization and the intercell coupling in order to achieve a cancellation for Eq. (18). If implemented with two-dot cells, the coupling between the control qubit causes further difficulties. Thus it seems to be reasonable to realize universal quantum computing [14,21–23] instead of the Deutsch gate with the set of single-qubit gates presented in the preceding section and the $\hat{U}_{zz, \varphi}^{(j, j+1)}$ gate. [$\hat{U}_{zz, \varphi}^{(j, j+1)}$ denotes the time evolution of the register with zero bias polarization, high barriers, and all intercell couplings switched off except for the coupling between the j th and $(j+1)$ th cell. Switching off the intercell couplings is possible with sequences of 180° pulses rotating around x as

is done for NMR [13]. When using two-dot cells, the pulse sequences become more complicated because of the more couplings to be eliminated.] The execution time of the multi-qubit gates (two-qubit conditional rotation around x , controlled NOT [14]) based on a sequence of single-qubit gates and $\hat{U}_{zz, \varphi}^{(j, j+1)}$ is around T_{coupling} and the requirements on the accuracy of control parameters are less strict.

V. DISCUSSION

It is instructive to compare the CQCA quantum computer to the nuclear spin quantum computers [10–19]. The role of the nuclear spin is now played by the coherence vector. The spin of the nucleus is manipulated by a strong constant magnetic field and a weaker alternating one while the CQCA uses external electrodes to control the interdot tunneling barriers. In the case of a spin quantum computer, there is a spin-spin coupling while the CQCA cells are coupled Coulombically. The classical analogy of the spin- $\frac{1}{2}$ system is a magnetic dipole. The classical analogy of a CQCA cell is an electric quadrupole (or for two-dot cells, a dipole). In nuclear or electron spin quantum computing, manipulating individual qubits is rather difficult. The NMR devices are running an ensemble of parallel quantum computers. A related approach [26,27,32] uses the electron spin in a quantum dot for a qubit, but writing data in and reading data out seems to be technologically very difficult. The technology for writing into and reading out of the individually accessible CQCA cells is already available [65].

Nuclear and electron spin seem to be ideal candidates for two-state systems. Most other implementations suffer from the problem of the possibility of exciting parasitic, noncomputational energy levels (“leakage” [66]). In a CQCA register, the intercell coupling and tunneling can be much smaller than the level spacing of the quantum dot. Thus to get to noncomputational parasitic states requires much more energy than the energy difference between the computational states, unlike in the case of proposals, where the information is stored in the ground state and the first excited state of the electron in the quantum dot.

The limiting factor in the CQCA approach is the shorter decoherence time, which restricts the number of quantum operations. The issue of dephasing in open quantum dots has been addressed in the literature [67–70]. In Ref. [67], the dephasing time is measured in open ballistic GaAs quantumdots with areas between 0.4 and 4 μm^2 and single-mode point contacts. Measurements between $T=0.34$ and 4 K show that the dephasing time is independent of the dot area and it has both a T^{-1} and T^{-2} dependence, with a saturation at low temperatures. For $T=3$ K, the dephasing time is around 2.4 ns. (A T^{-2} dependence is expected for isolated dots for intermediate temperatures [71–73].)

It must be noted that the dot size proposed for QCA [41,56–59] is much smaller than in the experiments mentioned above. Due to the small dot size, the mean level spacing of the quantum dot is much larger than kT . ($\Delta = 2\pi\hbar^2/m^*A = 72 \text{ meV} = 824 \text{ K}$ for a GaAs dot with an area $A = 100 \text{ nm}^2$.) References [28] and [29] model a quantum-dot structure of dots with 4-nm diam. Considering only

acoustic-phonon–electron scattering, the dephasing time is obtained as a couple of nanoseconds for $T=10$ K. It is also an important conclusion of the papers that by choosing the state and the physical parameters properly, the dephasing can be largely suppressed in a quantum-dot array.

Dephasing in double dots was also studied [74–77]. Reference [77] determines the relaxation time for two Coulombically coupled double dots (cell size 60 nm), considering also only electron–acoustic-phonon scattering. For damping rate, 0.15 GHz = 1/6.7 ns is obtained [78]. For the particular structure, E_0 was 0.62 meV. This value for E_0 is consistent with other calculations [41]. In order to get substantially larger intercell electrostatic coupling, one must enter the molecular regime. This limit is true for both the coupling between double dots and between the two-double-dot cells. As was stated before, a cell can be considered a two-state system only if both the tunneling energy and the E_0 intercell coupling are smaller than the coupling energy between the doubled dots. In order to have two-state four-dot cells, one must decrease the strength of the intercell coupling much below the achievable limit, which seems to be unreasonable. Thus a two-dot cell is much more feasible for quantum computing.

The time that is necessary for the intercell coupling to affect the dynamics considerably is $T_{\text{coupling}} = \hbar/E_0$. Assuming $E_0 = 1$ meV, $T_{\text{coupling}} = \hbar/E_0 \approx 1$ ps. According to Eq. (13), the duration for the NOT operations is $T = \hbar \pi / 2 \gamma$. It is smaller by several orders of magnitude than T_{coupling} , because $\gamma \gg E_0$. The same is true for all the single-qubit gates. A multi-qubit gate has an execution time near T_{coupling} . Since there is a three orders of magnitude difference between the low-temperature dephasing time in quantum dots and the ex-

ecution time of a multi-qubit operation, we can at least say that the relatively short decoherence time does not seem to prohibit the application of quantum-dot cellular automata for quantum computing [79]. We note that two crucial questions concerning the feasibility of CQCA quantum computing must be distinguished. The first is whether a large quantum register can be realized with CQCA in the future. The second is whether a system with a few qubits can be realized with the present or near-future technology. Even if large-scale implementation proves to be difficult, CQCA technology can still be used as a tool to test the concepts of quantum computing in solid-state devices.

VI. CONCLUSIONS

We have proposed a multiple-quantum-dot structure—Quantum cellular automata (QCA)—as a mode of realizing quantum computing. Basic operations can be performed with a line of QCA cells; a universal quantum computer can be constructed. QCA may offer an example of an integrable quantum computer with electrostatic data read-in/write-out. The main drawback of this implementation is the relatively short decoherence time compared to the implementations using nuclear or electron spins.

ACKNOWLEDGMENTS

We are very grateful to John Timler, Árpád Csurgay, and the participants of the TMR Network School on Quantum Computation and Quantum Information Theory (Torino, July, 1999) for stimulating discussions. This work was supported by the office of Naval Research MURI program.

-
- [1] C. P. Williams and Scott H. Clearwater, *Explorations in Quantum Computing* (Springer, New York, 1998).
 - [2] A. Steane, e-print quant-ph/9708022.
 - [3] R. P. Feynman, *Int. J. Theor. Phys.* **21**, 467 (1982).
 - [4] D. Deutsch, *Proc. R. Soc. London, Ser. A* **400**, 97 (1985).
 - [5] D. Deutsch, *Proc. R. Soc. London, Ser. A* **425**, 73 (1989).
 - [6] S. Lloyd, *Science* **261**, 1569 (1993).
 - [7] L. K. Grover, *Phys. Rev. Lett.* **79**, 325 (1997).
 - [8] D. P. DiVincenzo, *Phys. Rev. A* **51**, 1015 (1995).
 - [9] D. P. DiVincenzo, *Nature (London)* **393**, 113 (1998).
 - [10] N. Gershenfeld and I. L. Chuang, *Sci. Am.* **1998**, 66.
 - [11] I. L. Chuang, N. Gershenfeld, and M. Kubinec, *Phys. Rev. Lett.* **80**, 3408 (1998).
 - [12] I. L. Chuang, L. M. K. Vandersypen, X. Zhou, D. W. Leung, and S. Lloyd, *Nature (London)* **393**, 143 (1998).
 - [13] D. G. Cory, R. Laflamme, E. Knill, L. Viola, T. F. Havel, N. Boulant, G. Boutis, E. Fortunato, S. Lloyd, R. Martinez, C. Negreverenge, M. Pravia, Y. Sharf, G. Teklemariam, Y. S. Weinstein, and W. H. Zurek, e-print quant-ph/0004104.
 - [14] D. G. Cory, Mark D. Price, and Timothy F. Havel, *Physica D* **120**, 82 (1998).
 - [15] T. Sleator and Harald Weinfurter, *Phys. Rev. Lett.* **74**, 4087 (1995).
 - [16] J. A. Jones, M. Mosca, and R. H. Hansen, *Nature (London)* **393**, 344 (1998).
 - [17] R. Marx, A. F. Fahmy, J. M. Myers, W. Bermel, and S. J. Glaser, e-print quant-ph/9905087.
 - [18] N. Linden, E. Kupce, and R. Freeman, *Chem. Phys. Lett.* **311**, 321 (1999).
 - [19] E. Knill, R. Lflamme, R. Martinez, and C.-H. Tseng, *Nature (London)* **404**, 368 (2000).
 - [20] B. E. Kane, *Nature (London)* **393**, 133 (1998).
 - [21] A. Barenco, D. Deutsch, A. Ekert, and J. Jozsa, *Phys. Rev. Lett.* **74**, 4083 (1995).
 - [22] A. Barenco, B. Benett, R. Cleve, D. P. DiVincenzo, N. Margolus, P. Shor, T. Sleator, J. A. Smolin, and H. Weinfurter, *Phys. Rev. A* **52**, 3457 (1995).
 - [23] A. Barenco, e-print quant-ph/9505016.
 - [24] R. Marx, A. F. Fahmy, J. M. Myers, W. Bermel, and S. J. Glaser, e-print quant-ph/9905087.
 - [25] L. A. Openov, e-print cond-mat/9906390.
 - [26] G. Burkhard, D. Loss, and D. P. DiVincenzo, *Phys. Rev. B* **59**, 2070 (1999).
 - [27] G. Burkhard and D. Loss, *Phys. Rev. B* **60**, 11 404 (1999).
 - [28] P. Zanardi and F. Rossi, *Phys. Rev. Lett.* **81**, 4752 (1998).
 - [29] P. Zanardi and F. Rossi, *Phys. Rev. B* **59**, 8170 (1999).

- [30] G. D. Sanders, K. W. Kim, and W. C. Holton, *Phys. Rev. A* **60**, 4146 (1999).
- [31] T. Tanamoto, e-print quant-ph/990231.
- [32] D. Loss and D. P. Vincenzo, *Phys. Rev. A* **57**, 120 (1998).
- [33] P. Shor, *Proceedings of the 35th Annual Symposium on Foundations of Computer Science* (IEEE Press, Santa Fe, New Mexico, 1994), pp. 124–134.
- [34] J. Cirac and P. Zoller, *Phys. Rev. Lett.* **74**, 4091 (1995).
- [35] Q. Turchette, C. Hood, W. Lange, H. Mabuchi, and H. Kimble, *Phys. Rev. Lett.* **75**, 4710 (1995).
- [36] L. Grover, in *Proceedings of the 28th Annual ACM Symposium on the Theory of Computing* (IEEE Press, Philadelphia, PA, 1996), pp. 212–219.
- [37] Y. Nakamura, YuA. Pashkin, and J. S. Tsai, *Nature* (London) **398**, 786 (1999).
- [38] L. B. Ioffe, V. B. Geshkenbein, M. V. Feigel'man, A. L. Fauchere, and G. Blatter, *Nature* (London) **398**, 679 (1999).
- [39] Y. Makhlin, G. Schön, and A. Shnirman, *Nature* (London) **398**, 305 (1999).
- [40] A. Shnirman and G. Schön, *Phys. Rev. B* **57**, 15 400 (1998).
- [41] C. S. Lent, P. D. Tougaw, W. Porod, and G. H. Bernstein, *Nanotechnology* **4**, 49 (1993).
- [42] C. S. Lent, P. D. Tougaw, and W. Porod, *Appl. Phys. Lett.* **62**, 714 (1993).
- [43] C. S. Lent and P. Douglas Tougaw, *J. Appl. Phys.* **74**, 6227 (1993).
- [44] P. Douglas Tougaw and C. S. Lent, *J. Appl. Phys.* **75**, 1818 (1994).
- [45] C. S. Lent and P. D. Tougaw, *J. Appl. Phys.* **75**, 4077 (1994).
- [46] C. S. Lent, P. Tougaw, and W. Porod, *PhysComp '94: Proceedings of the Workshop on the Physics of Computing* (IEEE Computer Society Press, Dallas, TX, 1994), pp. 5–13.
- [47] G. Tóth, C. S. Lent, P. D. Tougaw, Yu. Brazhnik, W. Weng, W. Porod, R. Liu, and Y. Huang, *Superlattices Microstruct.* **20**, 463 (1996).
- [48] C. S. Lent, P. Tougaw, and W. Porod, *J. Appl. Phys.* **80**, 4722 (1996).
- [49] C. S. Lent and P. D. Tougaw, *Proc. IEEE* **85**, 541 (1997).
- [50] G. Tóth and Yu. Brazhnik (unpublished).
- [51] A. O. Orlov, I. Amlani, G. H. Bernstein, C. S. Lent, and G. L. Snider, *Science* **277**, 928 (1997).
- [52] A. O. Orlov, I. Amlani, G. Tóth, C. S. Lent, G. H. Bernstein, and G. L. Snider, *Appl. Phys. Lett.* **73**, 2787 (1998).
- [53] T. Dittrich, P. Hänggi, G.-L. Ingold, B. Kramer, G. Schön, and W. Zwenger, *Quantum Transport and Dissipation* (Wiley-VCH Verlag, Germany, 1998). Chapter 3 summarizes single-electron tunneling.
- [54] The bias gates are new compared to the noncoherent QCA applications. They are introduced here since at least two control parameters per cell are necessary to be able to construct all the possible single-qubit operations.
- [55] For example, when a single cell is oscillating between the two computational states while the barriers are low, $E_{DD}/t = 10$ (20) reduces the probability of the parasitic states to 7% (2%). It is also possible that there are other, more complicated schemes that use only a two-dimensional subspace for a QCA cell. Reference [47] presents such a scheme for a QCA cell line with a constant interdot barrier height used for classical digital computing. A 16-dimensional space is used to describe the state of the particular QCA cell introduced there, however during the dynamics the cell remains in a two-dimensional subspace to a very high degree of accuracy.
- [56] Y. Fu and M. Willander, *J. Appl. Phys.* **83**, 3186 (1998).
- [57] I. I. Yakimenko, I. V. Zozoulenko, C.-K. Wang, and K.-F. Berggren, *J. Appl. Phys.* **85**, 6571 (1999).
- [58] H. Wu and D. W. L. Sprung, *J. Appl. Phys.* **84**, 4000 (1998).
- [59] M. Governale, M. Macucci, G. Iannaccone, C. Ungarelli, and J. Martonell, *J. Appl. Phys.* **85**, 2962 (1999).
- [60] G. Tóth, J. Timler, and C. S. Lent, in *Proceedings of the IEEE International Workshop on Computational Electronics (IWCE-6)* (IEEE Press, Osaka, 1998), pp. 42–45.
- [61] G. Mahler and V. A. Weberruß, *Quantum Networks* (Springer, Berlin, 1995).
- [62] The following deduction is for four-dot cells, but it can be straightforwardly extended to double-dot cells by including next-to-nearest-neighbor couplings, or alternatively these couplings can be canceled by additional operations inverting some of the qubits, as is done for NMR [13].
- [63] In the general case, the backaction of the qubit on the neighbors should also be considered, however in the case of the quantum gates presented in Sec. IV, the neighboring cells have high barriers, thus their polarization and consequently E_{Σ} do not change. The dynamical equation (11) for the coherence vector is coupled to the neighbors only through E_{Σ} , thus including backaction explicitly in the model would not give a different dynamics for the coherence vector.
- [64] For the multi-qubit gate described in the beginning of Sec. IV, $\vec{\Gamma}$ does not have a z component if the polarizations of the two neighbors are such that $E_{\Sigma} = 0$. In this case, the terms in Eq. (18) cancel each other. In reality, the third coordinate of $\vec{\Gamma}$ is not zero, but it must be much smaller than the first: $E_{\Sigma} = E_0(P_{\text{left}} + 2P_{\text{right}} + P_{\text{bias}}) \ll \gamma$. For a multi-qubit operation, $\gamma \ll E_0$. Combining the two inequalities and dividing by E_0 leads to $P_{\text{left}} + 2P_{\text{right}} + P_{\text{bias}} \ll \gamma/E_0 \ll 1$. Thus for the error of the bias, $\Delta P_{\text{bias}} \ll \gamma/E_0 \ll 1$ is required. There is a similar requirement for the accuracy of the E_j intercell coupling.
- [65] R. R. Ernst, G. Bodenhausen, and A. Wokaun, *Principles of Nuclear Magnetic Resonance in One and Two Dimension* (Clarendon, Oxford, 1987).
- [66] R. Fazio, G. M. Palma, and J. Sienwert, *Phys. Rev. Lett.* **83**, 5385 (1999).
- [67] A. G. Huibers, M. Switkes, C. M. Marcus, K. Capman, and A. C. Gossard, *Phys. Rev. Lett.* **81**, 200 (1998).
- [68] A. G. Huibers, J. A. Folk, S. R. Patel, C. M. Marcus, C. I. Duruöz, and J. S. Harris, Jr., *Phys. Rev. Lett.* **83**, 5090 (1999).
- [69] R. M. Clarke, I. H. Chan, C. M. Marcus, C. I. Duruöz, J. S. Harris, Jr., K. Campman, and A. C. Gossard, *Phys. Rev. B* **52**, 2656 (1995).
- [70] J. P. Bird, K. Ishibashi, D. K. Ferry, Y. Ochiai, Y. Aoyagi, and T. Sugano, *Phys. Rev. B* **51**, 18 037 (1995).
- [71] U. Shivan, Y. Imry, and A. G. Aronov, *Europhys. Lett.* **28**, 115 (1994).
- [72] Y. M. Blanter, *Phys. Rev. B* **54**, 12 807 (1996).
- [73] B. Altshuler, Y. Gefen, A. Kamenev, and L. S. Levitov, *Phys. Rev. Lett.* **78**, 2803 (1997).
- [74] R. H. Blick, D. Pfannkuche, R. J. Haug, K. v. Klitzing, and K. Eberl, *Phys. Rev. Lett.* **80**, 4032 (1998).
- [75] T. Schmidt, R. J. Haug, K. v. Klitzing, A. Förster, and H. Lüth,

- Phys. Rev. Lett. **78**, 1544 (1997).
- [76] P. Boucaud, K. S. Gill, J. B. Williams, M. Sherwin, W. V. Schoenfeld, and P. M. Petroff, Appl. Phys. Lett. **77**, 510 (2000).
- [77] A. Yu. Smirnov, N. J. M. Horing, and L. G. Mourokh, J. Appl. Phys. **87**, 4525 (2000).
- [78] The damping rate calculations were done for intermediate barrier height and around the steady state.
- [79] The problem of controlling gates on fast time scales may in fact limit the speed of computing and lead to a smaller number of possible operations. That issue is primarily concerned with designing capacitances.